Reverse movement and coalescence of water microdroplets in electrohydrodynamic atomization

L. L. F. Agostinho,[1,2] E. C. Fuchs,[1] S. J. Metz,[1] C. U. Yurteri,[2] and J. C. M. Marijnissen[1,2]
[1]*Wetsus Centre of Excellence for Sustainable Water Technology, Agora 1, NL-8900 CC Leeuwarden, The Netherlands*
[2]*Faculty of Applied Sciences, Delft University of Technology, NL-2628 BL Delft, The Netherlands*
(Received 15 March 2011; published 15 August 2011)

When a high voltage is applied to a liquid pumped through a needle, charged microdroplets can be formed, which are carried along the electric field lines. This phenomenon is called electrohydrodynamic atomization (EHDA), or simply electrospray. In this work we show that in the case of water, droplets may reverse their paths flying back toward the liquid meniscus, sometimes making contact with it. Such reverse movement is caused by polarization of the water inside the strong electric field. To understand this phenomenon we developed a way to calculate the droplet charge using its trajectory obtained by high-speed imaging. The values found showed that these droplets are charged between 2.5% and 19% of their Rayleigh limit.

DOI: 10.1103/PhysRevE.84.026317 PACS number(s): 47.65.−d

I. INTRODUCTION

Electrohydrodynamic atomization (EHDA), or simply electrospray, is a physical process that concerns the disruption of a liquid into a spray of charged droplets when it is subjected to an intense electric field (EF). The history of electrospray research dates back to the late 16th century when William Gilbert discovered that, in the presence of a charged piece of amber, a drop of water deformed into a cone [1]. Almost 300 years later Lord Rayleigh estimated the maximum amount of charge a liquid droplet could carry [2,3] based upon equilibrium between electrostatic repulsion and surface tension, the so-called Rayleigh limit. In the early 20th century, Zeleny published two important works about electrified liquid surfaces [4,5], and in the 1960s, Taylor paved the way for modern electrohydrodynamics (EHD) [6]. Examples of EHD-based technologies include electrospray-ionization mass spectroscopy (ESI-MS) [7] and the production of particles for medical and agricultural purposes [8–10]. A good overview of the field is given in the book by Bailey [11], in the review by Grace and Marijnissen [12], and in the work of Eggers and Villermaux [13]. The different kinds of electrosprays generated under different conditions are classified as "spray modes." The classification and characteristics of the different modes in EHDA are topics extensively explored by many authors [12,14–18]. Based on the reported classifications, we could identify that the phenomenon reported in this work was observed in a regime between the dripping and the cone-jet mode, which can be called a pulsating jet mode [12]. The mode is sometimes differentiated into a spindle mode and an intermittent cone-jet mode [12,15]. We will not go into further details, and we will refer to our spray as operating in a "pulsating jet" mode throughout the text.

The recent advances accomplished in the EHDA field are important not only for the development of the above-mentioned technologies but also because they trigger a whole new group of phenomena based on the interaction of liquids with strong electric fields. Among these phenomena one can mention the work of Fuchs *et al*. [19,20], who rediscovered Armstrong's [21] rope of water and published a series of papers about this "floating water bridge," the influences of EF on liquid-liquid coalescence [22–27], the work of Ristenpart *et al*. [28], who has reported on the noncoalescence of oppositely charged droplets immersed in strong EF, and the deformation of droplets immersed in strong electric fields [29,30]. The last three examples are especially important for the good understanding of this paper; and therefore will be better explored in the following paragraphs.

The influences of an external EF on liquid-liquid coalescence was probably first reported by Allan and Mason [26]. They claimed that the application of strong electric fields increases the ratio of coalescence due to induced charge polarization. The same authors later also investigated the coalescence of liquid droplets in electric and shear fields [24]. They observed that oppositely charged water droplets immersed in silicone oil repelled one another below a critical separation distance. The authors could not completely explain the phenomenon and said simply, based on the observation of some images, that the reason was probably an "electrical discharge" between the droplets.

Contrary to the assumption that EFs can enhance coalescence of droplets with opposite polarity, a recent report by Ristenpart *et al*. [28] showed that above a critical EF strength charge transfer can take place before coalescence happens, and the droplets, instead of coalescing, bounce off each other. After that, Bird *et al*. [25] investigated electrically driven coalescence and recoil of water droplets and claimed that the EF has an important role in distorting a droplet's surface prior to contact and also that the subsequent dynamics depend predominantly on capillary forces. Apart from the experiments done by Allan and Manson, the other authors investigated coalescence for very low droplet velocities (e.g., $v < 1\ \mathrm{m\ s^{-1}}$) only. Allan and Manson took inertia into account but still could not explain the bouncing effect completely.

Regarding the stability of droplets in an EF, it is known that these fields cause droplets to develop conical structures oriented along the direction of the field lines. Many authors investigated these effects both for charged and uncharged droplets [29–31]. Commonly referred to as *Taylor cones* [6], these structures result from a balance of charge-induced pressure from the applied EF and surface tension stresses resisting interfacial deformation [25]. In a situation where the physical characteristics of a droplet are constant (i.e., permittivity, surface tension, and radius), the field is the critical factor to define whether the droplet will be stable or not.

According to Grimm and Beauchamp [30], for critical values of the field, an uncharged single droplet will develop two opposing conical tips (prolate spheroidal shape) aligned with it. If the droplet is charged, instead of adopting a prolate spheroidal shape, it becomes distinctly tear shaped.

A direct consequence of these instabilities is the spraying of charged progeny droplets from the formed Taylor cones. Grimm and Beauchamp [30] also investigated the formation of these sprays. They found that neutral droplets exhibited the same prolate elongation mentioned by Brazier-Smith [29] with symmetric "cone jets" of positive and negative progeny droplets. Droplets with a net charge q take the form of asymmetric tear shapes and emit a single charged jet. According to the authors, sometimes the total charge loss can be greater than the original droplet charge, resulting in oppositely charged droplets. These instabilities, although apparently similar, cannot be directly related to the so-called droplet Rayleigh limit. Both phenomena assume the droplet's disruption to be a consequence of imbalance between the cohesive forces due to surface tension and the repulsive electrostatic forces. The last one is a consequence of droplet charge density, which surpasses a certain threshold, the Rayleigh limit. The first one, on the other hand, explains that the strong electric field induces charge migration (electrokinetic movements) inside the droplet, leading to some deformations on its spherical shape like the ones predicted by [30]. These deformations can, eventually, end up with droplet disruption. Consequently, the instabilities mentioned by Refs. [29–31] can be seen even when the droplet charge is way below its Rayleigh limit.

Bird *et al*. [25] suggested the nondimensional electrocapillary number $\varepsilon_c = \frac{\varepsilon\varepsilon_0 E^2 a}{\gamma}$, where $\varepsilon\varepsilon_0$ is the permittivity of the liquid, E is the magnitude of the electric field at droplet's surface, a is the droplet radius, and γ is the surface tension, to predict whether a droplet will deform or not when immersed in a certain electric field. The number represents the ratio between charge-induced pressure from the applied electric field and surface tension stress resisting interfacial deformation [25]. If this ratio is greater than 1, a liquid droplet will deform inside the field. In the same paper Bird *et al*. found that if $\varepsilon_c > 1.44$, two oppositely charged water droplets failed to coalesce. The explanation for this is, according to them, that at higher values of ε_c the droplets became unstable prior to contact, causing electrospraying [25], and that the electrospray would balance charges, causing the recoil. Due to these observations, they have concluded that electrospray may play an important role in the recoil of charged droplets.

In this study, we report the unexpected observation of a reverse movement of EHDA-produced water droplets back to the nozzle from which they were ejected. The phenomenon was observed in the pulsating jet mode. Considering that the returning of a sprayed droplet normally leads to contact between this droplet and the liquid meniscus, it is believed that this phenomenon can be used to better understand charged liquid-liquid coalescence and its implications. The importance of investigating the coalescence between droplet and meniscus under this specific situation is that, in addition to what has been reported in the literature, with EHDA we are able to verify whether droplet inertia also plays an important role in this situation or not.

II. EXPERIMENT

A. Electrospray configuration

Electrospraying of water was studied using a capillary-plate configuration with variable nozzle to plate distances, i.e., between 2 and 4 cm (see Fig. 1). A blunt ended, polished, stainless steel needle (FED, Inc.) was used as a nozzle (gauge number 22, 410 μm inner diameter and 710 μm outer diameter, uncoated). A syringe pump type SP-12S PRO AITEC was used to deliver the liquid to the nozzle. The flow rate was also variable but was generally established around 2 mL h^{-1}. High voltage was applied with a FUG HCP 35–35000 DC high voltage power supply. In some experiments the counter electrode (steel plate 4 × 4 cm^2) was subjected to a high voltage (negative) with the nozzle grounded; in other experiments the nozzle was subjected to a high voltage (positive) with the counter electrode grounded. Configurations

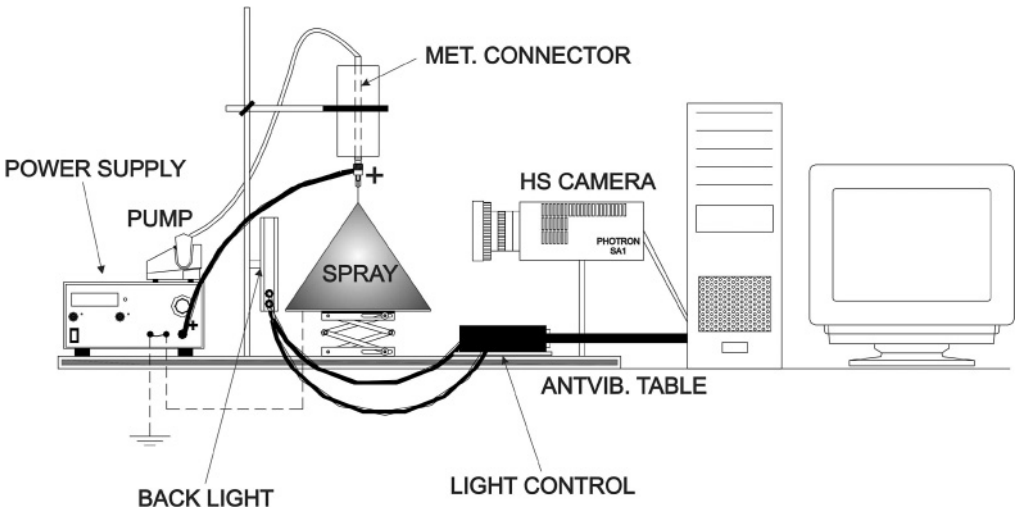

FIG. 1. Electrospray and optical system scheme.

were always defined in order to allow the formation of positive droplets in the pulsating jet mode [12,15,32–35]. The liquid used was deionized water (∼18 MΩ cm, Millipore). When required, simulations were done with the electrostatics module of the Comsol® MULTIPHYSICS software bundle. In some cases the spray currents were measured using a 1 MΩ resistor (5% tolerance), which was placed between the ground and the nozzle (with the potential applied on the counter electrode). To synchronize the electric current signal with the recorded movies a CONTEC (16 channels) data acquisition board and a RIGOL oscilloscope DS1022C (not represented in Fig. 1) were used.

B. Optical system

An optical system consisting of a high speed (HS) camera (Photron SA-1) and diffused backlight illumination (Microscope light source Karl Storz Technolight 270 with liquid light guide and diffuser) was used to record the experiments (see Fig. 1). IMAGEJ® was used for image processing; brightness and contrast corrections were done using Corel PHOTOPAINT® 15. All experiments were performed under ambient conditions at a temperature of ∼23°C and ∼55% relative humidity.

III. RESULTS AND DISCUSSION

A. Electrospray characteristics, droplet charge, and velocity

Under the experimental conditions different electrospray (ES) modes were observed using a constant flow rate while increasing the applied voltage. Due to the high surface tension of water it was not possible to reach a stable cone-jet mode. Therefore, the experiments were done in the pulsating jet mode. The basis of this classification is already addressed in the Introduction. In the pulsating jet mode we observed some unexpected phenomena, which will be described in this paper divided in three different categories. We saw some droplets returning (bouncing) to the meniscus and being completely reintegrated to it. This category will be called the returning followed by "complete coalescence" (category C1).

Figure 2 shows an example of the situation. The sequence starts with the meniscus assuming a conical shape (frame 1) from which a jet emerges and is atomized into fine droplets (frames 2–9). The jet starts to elongate, and a liquid ligament is formed (frames 10–12). This ligament is then detached from the meniscus (frame 13) and subsequently breaks up into droplets bigger than the previous ones (frames 14–16). These droplets descend due to gravity and electric forces

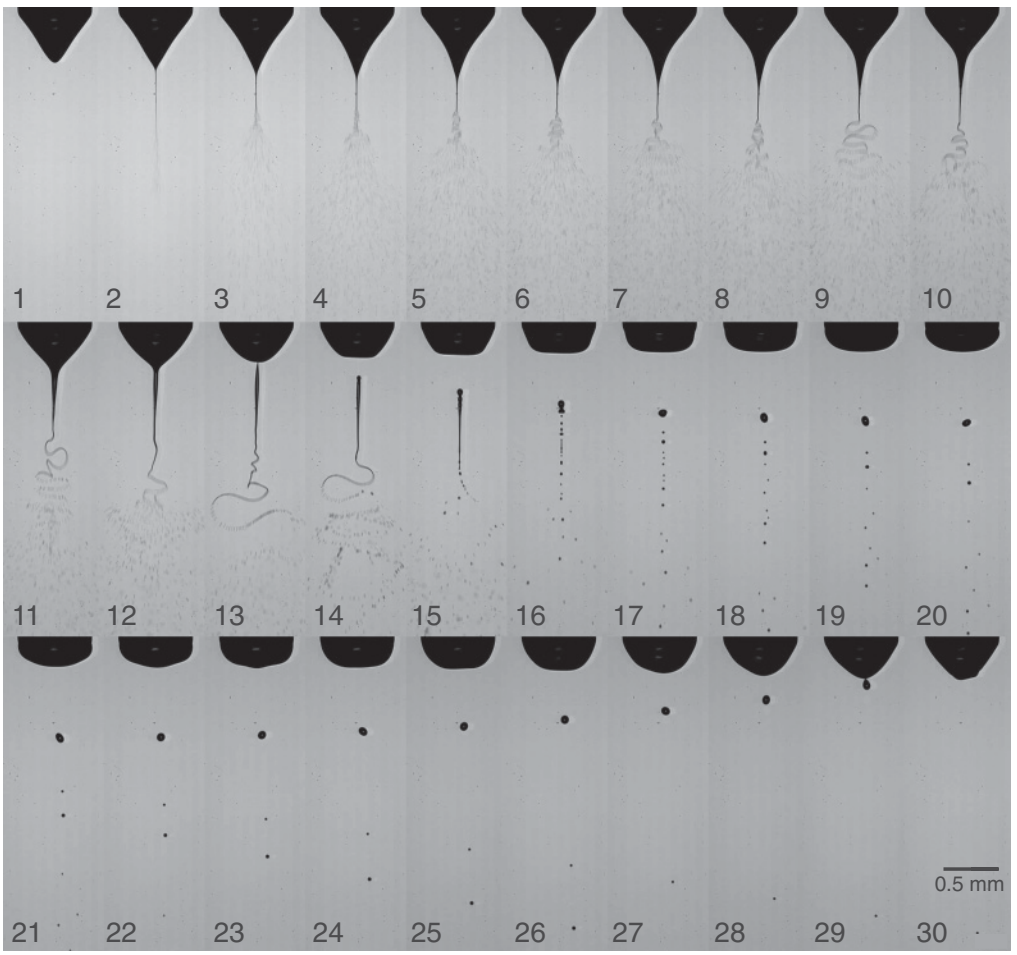

FIG. 2. Category C1 (complete coalescence): a droplet returns to the cone after being formed from a liquid ligament. The diameter of the returning droplet is ∼80 μm, the time frame between images is ∼45 μs, the applied potential is −5.67 kV on the counter electrode, and the flow rate used is 1 mL h^{-1}.

(frames 17–20), but the uppermost droplet reverses its path (frames 21–28) and collides with the meniscus (frame 29), where they coalesce (frame 30).

When considering the physical parameters of this experiment, the reverse movement of a droplet is most probably due to electrostatic attraction, which is only possible if this returning droplet is negatively charged. But since the potential applied on the nozzle is positive, only positive droplets thus are expected. A polarization of the liquid ligament by the strong electric field is the most plausible assumption and also justifies why the phenomenon was seen in the pulsating jet mode only, where long ligaments are created (see Fig. 3). Checking the literature we found that charging by polarization of water was already reported at the end of the 19th century by Lenard [36]. He was probably the first scientist to report the accumulation of positive and negative charges on water droplets in nature next to water falls. Also, Blanchard [37] observed that bubbles bursting over the ocean release positively charged droplets. It is important to remark that both situations do not happen in the presence of a strong electric field, just the normal field found on Earth, and still both authors have related the phenomena to charge separation on air-water interfaces. More recently, Maze *et al*. [38] reported the existence of negative droplets created by positive electrosprays from purified water. However, they do not elaborate on in which mode they were spraying. They have also considered that polarization would explain the existence of these negative droplets.

Figure 3 gives an overview of the mentioned charging mechanism. After detaching from the meniscus the liquid ligament becomes polarized, causing the end nearest the nozzle to assume an opposite charge (Fig. 3, left). Thus, the droplet(s) forming on this side may eventually carry less total charge or even opposite charge when compared to the charge of the initial ligament and the charge of the meniscus (Fig. 3, right).

It must be taken into account that polarization requires charge carriers to create a bipolar jet prior to breakup. However, the species that are actually transported in EHDA still lead to a topic not very well understood [39]. Many authors have reported on these carriers, but none of the presented theories are well accepted so far. Regardless of the inconsistencies normally found about this matter, some attempts to verify the nature of these charges were done. Polarization could be caused by electroconvection of H_3O^+ and OH^- under the strong electric field. As the liquid used in all experiments was deionized water, these would be the possible ionic entities to consider inside the liquid. The formation of hydronium cations solvated in water is known by self-ionization of water [40] and can be enhanced in the presence of strong electric fields [38]. One way to verify this in the time frame of the event is by checking how long the ligament persists in the electric field before it breaks up into droplets. A stable lifetime of $\sim$90 μs was calculated from the video capture frame rate. If it is assumed that H_3O^+ and OH^- are charge carriers inside the droplet, one can conclude that, due to their high mobility [41], this period is long enough to allow migration inside the ligament. This possibility would also have implications in changing the pH of the sprayed water. Experiments were done to verify water pH values before and after spraying. The pH measurements were done with WTW pH probes (340i series). The pH of the liquid was measured immediately after and immediately before the experiments. A nozzle-ring configuration was used to measure the pH after the spray, and the sprayed liquid was collected through a glass funnel into a glass bottle. The bottle and funnel were replaced each time, and each experiment was done in triplicate to confirm the results. No evidence of a pH change was found within the detection range of the equipment used.

Additional charge carriers could also come from electrochemical reactions inside the nozzle. Some authors have investigated the presence of metal ions in ESI and have successfully demonstrated that these ions can be generated by such processes [42], e.g., 54 μg L^{-1} of iron. As part of the experiments presented, an analysis of the sprayed liquid was done with inductively coupled plasma optical emission spectrometry (Perkin-Elmer Optima 5300 DV) to investigate the presence of metallic ions originating from the nozzle and metallic connector (see Fig. 1). This analysis did not indicate the presence of these ions in the sprayed liquid above the

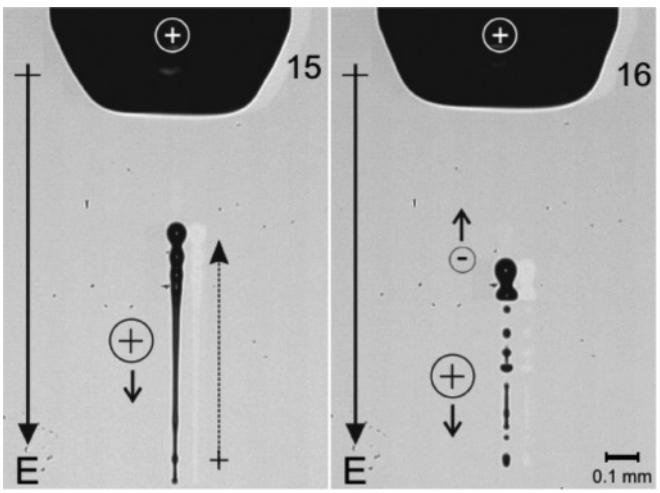

FIG. 3. Magnification of frames (left) 15 and (right) 16 from Fig. 2 showing the polarization of the aqueous ligament that subsequently forms differently charged droplets.

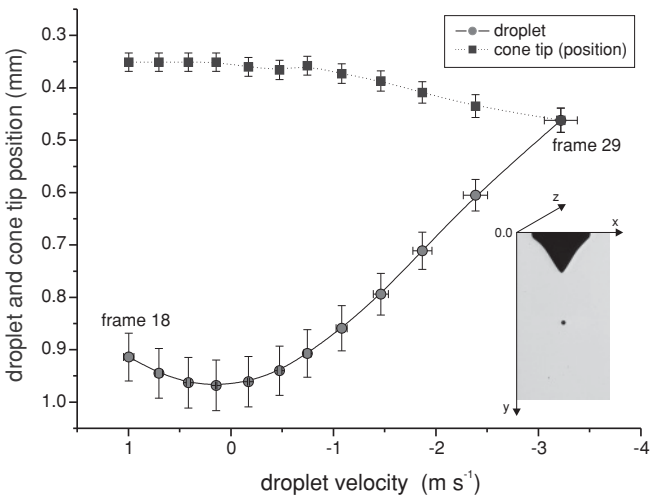

FIG. 4. Cone tip position, droplet axial coordinate against droplet velocity from frames 18 to 29, and coordinate system (returning droplet represented in Fig. 2).

detection threshold of the instrument (50 μg L^{-1} for Fe and 25 μg L^{-1} for Cr and Cu.

To verify whether the phenomenon would happen with other liquids under the same conditions we also performed experiments with mixtures of deionized water and NaCl (99% Sigma Aldrich) and deionized water and ethanol (Sigma Aldrich) at different concentrations. Experiments with these liquids have also shown some droplets returning toward the liquid meniscus but much less frequently than observed with deionized water only. This could be because deionized water has the right combination of physical properties to allow the formation of long ligaments inside the electric field. It is indeed observed that ligaments with deionized water are longer than ligaments with solutions of deionized water and NaCl and solutions of deionized water and ethanol.

Returning to Fig. 3, it is expected that after polarization takes place the returning droplet will be charged oppositely with respect to the meniscus. Because the generation of big droplets (over 50 μm) in pulsating modes is rather low, the returning droplet was almost always following its path toward the meniscus without interference from other nearby droplets. A possible interference could be created by a space charge, i.e., charged droplets sprayed before the ligament is formed. However, in many of the studied cases the returning droplet was formed long after the cone-jet phase of the pulsating spray, i.e., when the space charges are formed; thus this possibility was also disregarded. Later on, we will also mention that the space charges might be the reason that some droplets never came in contact with the meniscus (another studied case).

The nonexistence of extra droplets was seen as a good reason to try aerosol mechanics to calculate the charge of this droplet. If aerosol mechanics is to be used, droplet position, velocity, and trajectory must be known. Using high speed imaging these parameters were determined quite precisely and are presented in Fig. 4 (returning droplet represented on Fig. 2). By checking the droplet image's grey code it was possible to reduce the errors due to a possible movement perpendicular to the plane of observation (z axis). Nevertheless, a ~5% error is always expected due to the depth of field of the lens used.

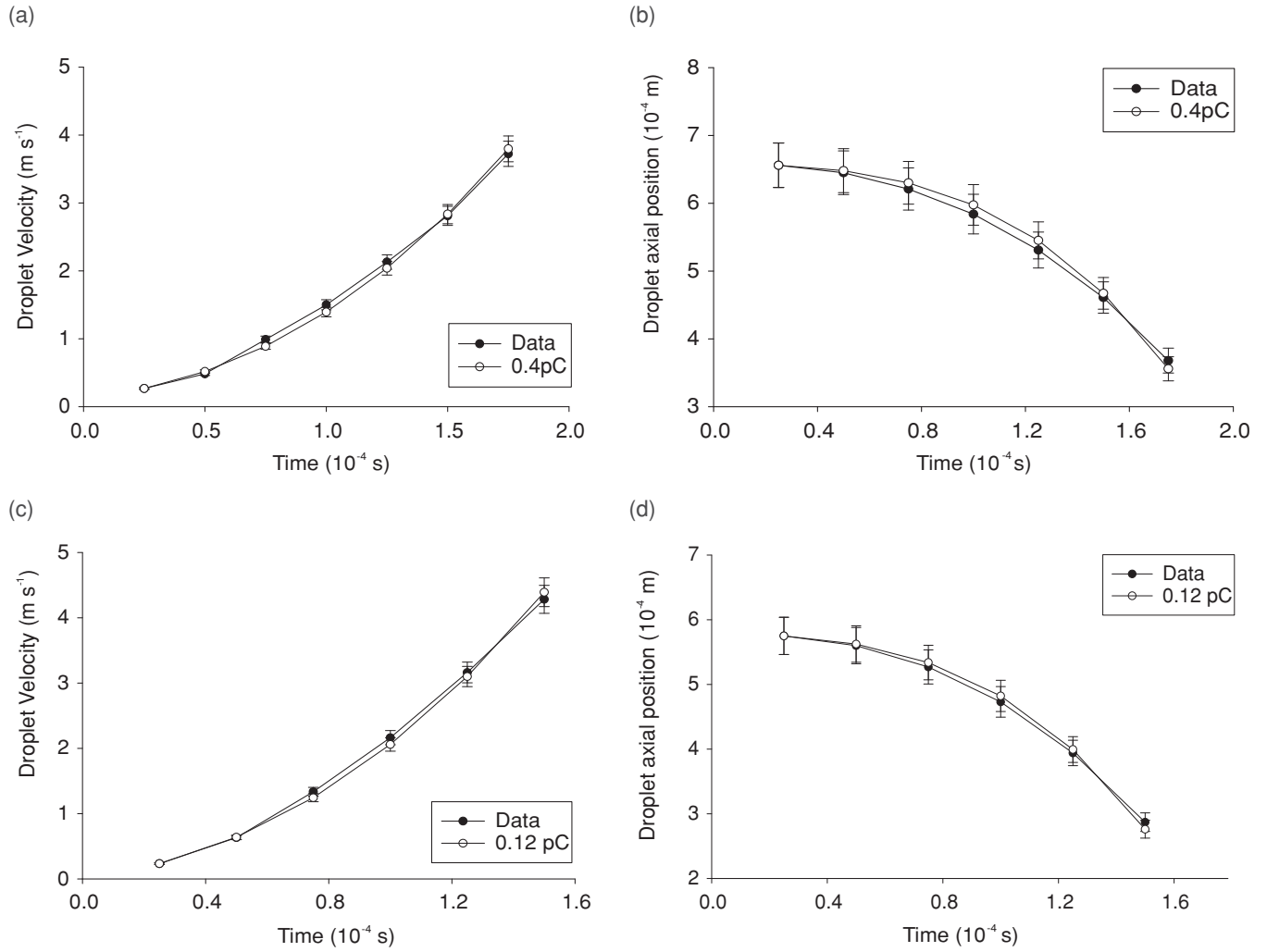

FIG. 5. Droplet velocities and axial position calculated from a sequence of frames and theoretically calculated correspondences for the same sequences. (a) and (b) The best fit found for a theoretical droplet charged with ~0.46 pC. (c) and (d) The best fit found for a theoretical droplet charged with ~0.12 pC. The potential used for both situations was 6 kV with 1 mL h^{-1} and 2-cm nozzle to plate distance.

B. Droplet charge calculation

The charge of the returning droplet was estimated from the experimentally observed trajectory using a vertical force balance. A critical parameter in this estimation was the electric field strength. The field close to the nozzle is particularly difficult to define for noncontinuous ES modes due to the dynamics of the meniscus. For the present situation the model was simplified by neglecting the time variance of the electric field. After assuming a certain stable shape for the meniscus coherent with the analyzed situation, the electric field strength was calculated using COMSOL Multiphysics.

A method combining HS imaging with a computer routine based on droplet momentum was used to calculate droplet charge. First, an image sequence of a returning droplet was chosen. To minimize the positional error caused by a possible movement of the droplet along the axis of observation, an initial routine selected droplets moving in the same plane by verifying their grey code. This also reduces the contribution from the radial component of the electric field. From the chosen set of images (Fig. 2) the droplet trajectory and diameter were then determined. The droplet velocity was calculated from the trajectory and the camera frame rate. To determine droplet charge another routine was used that modeled a "theoretical droplet" with the same diameter, initial position, and velocity, immersed in the same electric field as applied experimentally. In order to create an upward momentum, an electric attraction between the droplet and the meniscus is assumed. Then the droplet trajectory and velocity, assuming different charges, are calculated using charge quantities from 1 μC to 1 fC. The theoretical droplet trajectory and velocity are thus compared to the real droplet values, and the closest fit is chosen. In the present case, the best fits showed a deviation from the experiment of less than 5%. For these calculations the momentum conservation law applied to electrospray droplets [43] was used. Droplet-droplet interaction due to Coulombic effects was disregarded considering the distance of other droplets during the returning movement. The drag force was calculated according to Hinds [44], assuming a normal atmosphere and stable conditions. A droplet's mass was assumed to be constant in the studied trajectory, and deformations on a droplet's surface were neglected. Figure 5 shows the results obtained from this method for two different droplets of category C1.

C. Droplet charge and trajectory

The charge value adopted for a real droplet was the one that presented the best fit both for droplet axial position and droplet velocity. All selected droplets show an error smaller than 5% in relation to the fit. Figure 5 shows the comparison between measurement and model for the axial position and velocity of two different droplets with the adopted charge. Both cases are representative for bouncing with complete coalescence (C1). In the situation presented, the resultant droplet charges were 0.12 and 0.46 pC, respectively.

Overall, we found charges ranging between 0.32×10^{-13} C ($d \sim 30$ μm) and 8.0×10^{-13} C ($d \sim 90$ μm) for the droplets, as depicted in Fig. 6. Comparing the calculated droplet charge with the theoretical maximum charge a droplet can hold without disruption, the so-called Rayleigh limit, we found charges between 2.5% and 19% of this limit.

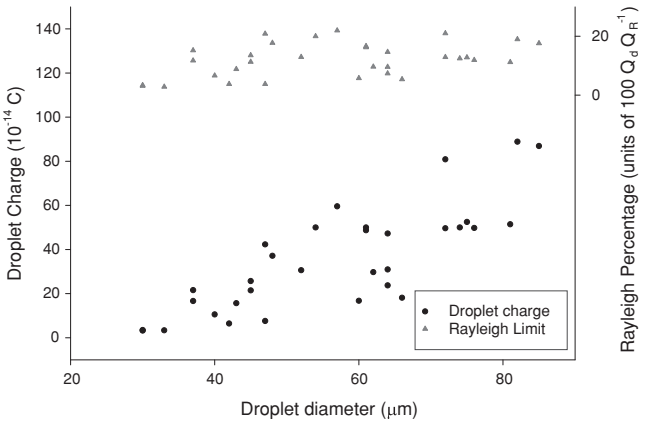

FIG. 6. Estimated droplet charges and respective percentage to Rayleigh limit for different diameters.

A charge far from the Rayleigh limit is expected for pulsating jet modes because these modes require relatively low potentials to be formed. There are no reported experimental values available in the literature to date to our knowledge that would provide data to compare with the presented results.

We observed a direct correlation between droplet charge and diameter, indicating that droplets with a higher diameter would carry more charge. This is an expected trend considering that a larger surface would allow a bigger quantity of charge.

Based on the measured diameter and calculated droplet charge we observed that droplets presented small variations on their surface charge density (SCD). This can be seen in Fig. 7, which shows droplet SCD against diameter, with an average SCD of 3.9×10^{-5} C m^{-2}.

D. Droplet interaction with the liquid meniscus

Until now we have explained a possible mechanism responsible for the return of a charged droplet against the electric

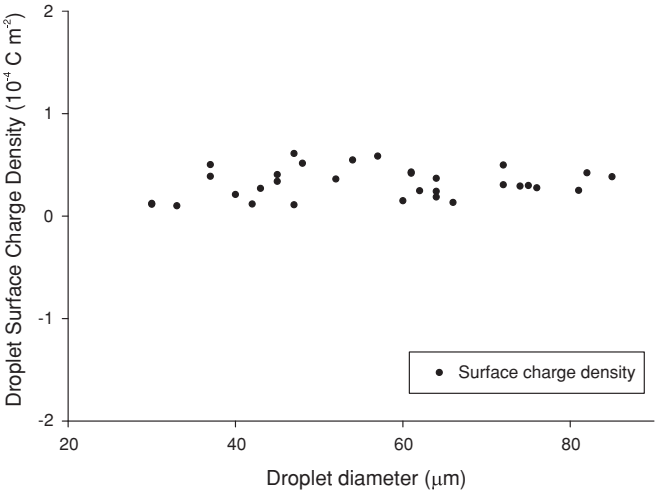

FIG. 7. Estimated droplet surface charge density for different diameters.

field and a possible way to calculate these droplets' charge. An observed consequence of this return is contact with the liquid meniscus. In such situations the contact is normally followed by coalescence between droplet and meniscus. However, as mentioned previously, two other situations have also been observed: In the second case, droplets reversed their path after being ejected from the nozzle, touched the meniscus, and were not completely reintegrated but just transferred part of their mass after the contact and then returned with a smaller radius. This interaction will be, therefore, called bouncing with "partial coalescence" (category C2).

The above interaction can be seen in Fig. 8. The sequence starts with the meniscus progressing from its spherical shape to a conical shape (frames 1–6). Some droplets from the previous cycle can be seen in the lower part of the image moving downward. From frame 7 to frame 10 the jet starts from the meniscus tip. From frame 11 to frame 14 the jet starts to whip on its lower part and is about to detach from the meniscus in frame 15. It is also visible that from frame 8 to frame 15 small droplets are produced on the tip of the jet. The ligament breakup begins in frame 16. From frame 16 to frame 28 the uppermost droplet is formed; it moves down, stops, and returns toward the meniscus. The droplet finally collides with the meniscus in frame 29, where it emits a spray of small droplets; in frame 30 it goes back downward with a smaller diameter.

In the third case, after the breakup, droplets decelerate as they move downward and stop. After remaining in equilibrium for some time they restart their downward movement. In rare cases some droplets, instead of just stopping, first decelerated, then stopped, then moved slightly upward, stopped again, and finally moved downward. But no good set of images to exemplify this last situation could be recorded. Because the droplet and meniscus are not in direct contact in this category, it will be called "noncoalescent" bouncing (category C3).

The sequence presented in Fig. 9 is a good example of category C3. The configuration applied was nozzle to plate, with 6 kV applied on the nozzle and a grounded plate placed 4 cm below.

In the first frame of this sequence the jet has already broken up, and the droplets are formed. From frames 2 to 6 one can see that all droplets below the uppermost one are going down following the field lines. From frames 1 to 17, the uppermost droplet is moving downward too. From frames 18 to 27 the droplet seems to be in "equilibrium"; its position is not changing with time. Starting with frame 27 (and continuing to frame 36), the droplet leaves its equilibrium and moves downward. It is also important to remark that the liquid meniscus assumes a conical shape in frame 21.

In order to better analyze this behavior, Fig. 10 shows the axial coordinate of the droplet in each frame for the whole sequence. There are three different phases of the

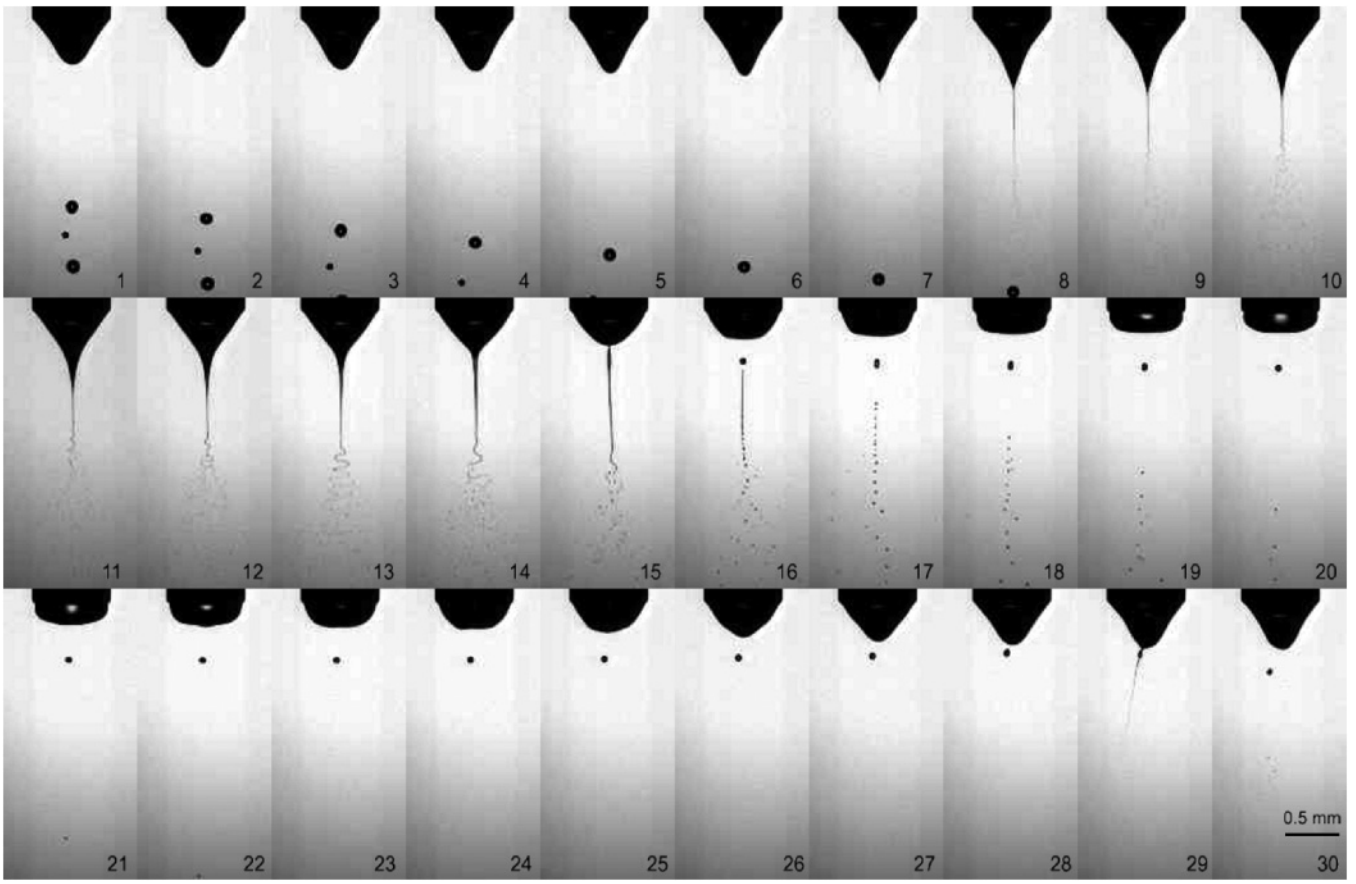

FIG. 8. Bouncing with "partial coalescence," or C2: a droplet collides with the meniscus with mass exchange. The droplet diameter before collision with the meniscus is ∼70 μm, and after it is ∼40 μm; the time frame between images is ∼50 μs, the applied potential is 5.0 kV on the nozzle, and the flow rate is 1 mL h^{-1}.

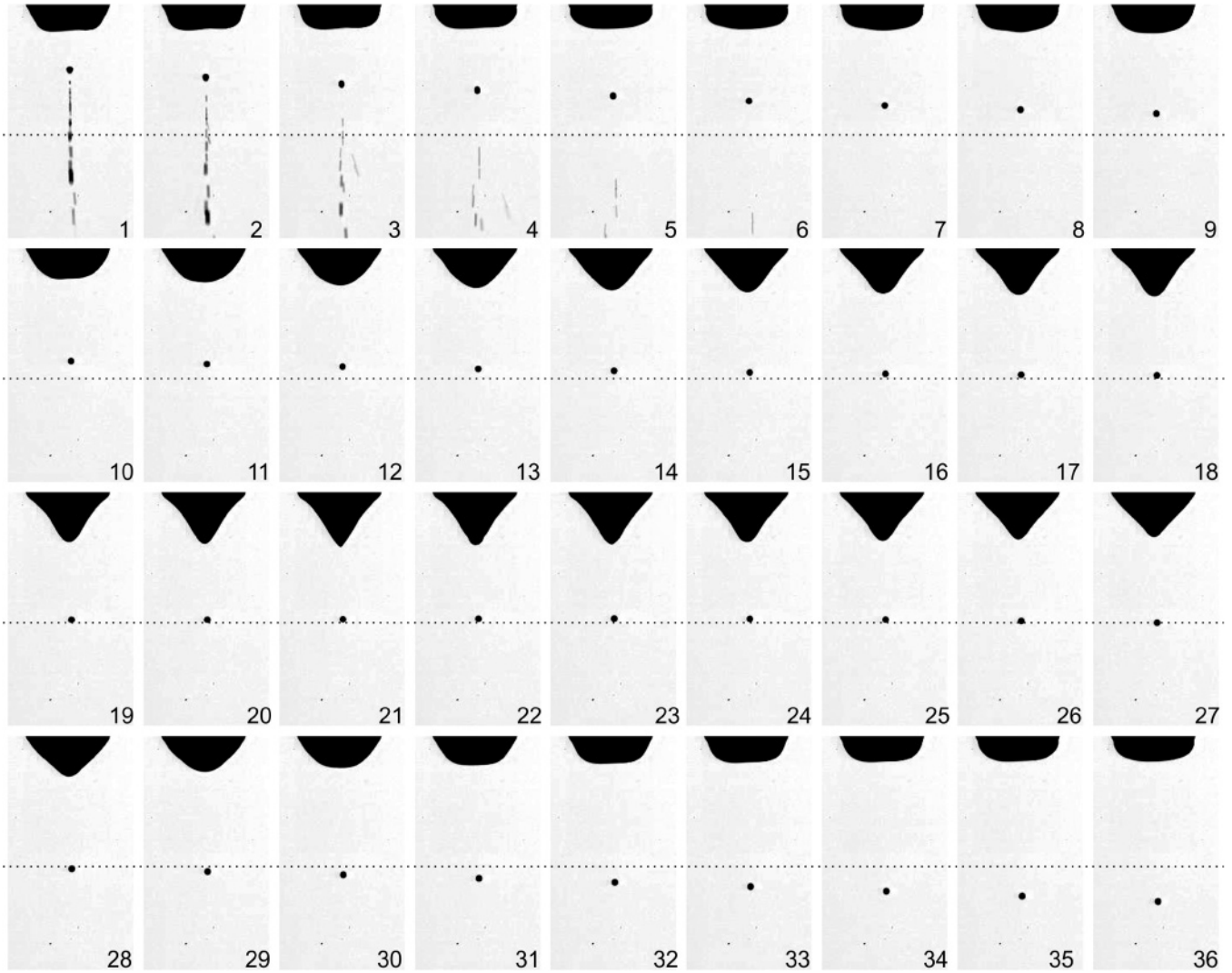

FIG. 9. Noncoalescent bouncing: nozzle to plate configuration with 6 kV applied on the nozzle. The plate was grounded and placed 4 cm below the nozzle. Dashed lines are arbitrarily placed to guide the eye. The droplet diameter is ~30 μm, and the time frame between images is 40 μs.

droplet's movement. First, from frames 1 to 17, the droplet is moving downward; from frames 18 to 27 the droplet's axial coordinate is not changing, corresponding to the equilibrium state mentioned before. After frame 27 the droplet continues its downward movement.

E. Comments on each category

We believe that the situations described above depend on polarization and in some cases also on charge transfer between droplet and meniscus. It is possible that not only is the applied electric field an important factor to consider in theses cases, as reported by [26,29,30], but so is the droplet's inertia. To better understand these different interactions we examined the stability of these droplets in the applied electric field, the coalescence phenomenon, and droplet mechanics.

Concerning droplet stability, it is known that from the shape assumed by the returning droplet during its movement, one can have a qualitative idea about its charge [26,29,30] before it contacts the meniscus.

Figure 11 shows a close look at different droplets, from different electrosprays, immediately before they touch the meniscus. The situations were all extracted from category C2 examples, which allowed us to observe the variations of the droplet shape. It is easy to see that all droplets deform into an asymmetric tear shape with the conical side pointing toward the meniscus. According to [30], this implies that they are charged oppositely in relation to the meniscus and corroborates our assumption that polarization is, in fact, inverting droplet charge during the ligament breakup.

To verify the role of droplet inertia in different categories we analyzed categories C1 and C2. Such analysis consisted in a random selection of droplets of these two categories followed by the calculation of their velocity and momentum from the breakup position until the moment immediately before they collide with the meniscus, i.e., the last frame with no contact. To assure that the situations were consistently comparable the droplets were extracted from the same electrospray, i.e., the same applied flow rate and the same electric field. Two different electrospray configurations were chosen for each

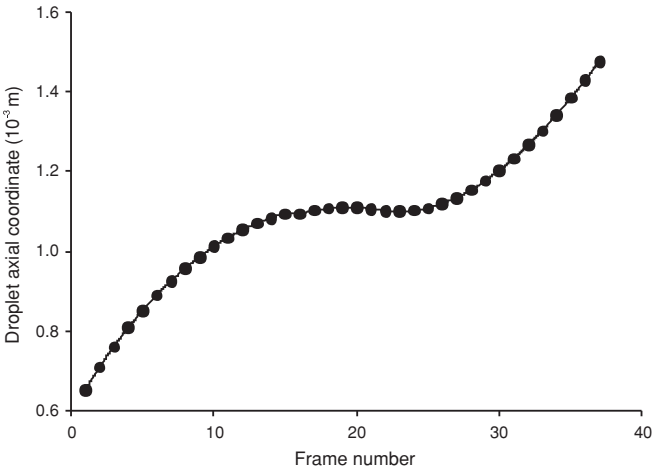

FIG. 10. Axial coordinate of the uppermost droplet represented in Fig. 9 against frame number. The chosen origin for the coordinate system is the same as in Fig. 4.

group of droplets, 0.5 mL h^{-1} with 6 kV and 2 mL h^{-1} with 5.5 kV applied to the nozzle. In both situations the nozzle to plate distance was 2.5 cm, and the spray mode was a pulsating jet mode.

Initially, we studied possible differences between the variation of droplet momentum against time for droplets in categories C1 and C2. Because C1 droplets were completely reintegrated and C2 droplets were only partially reintegrated, we first verified whether complete reintegration of C1 droplets could be attributed to a higher inertia. One can see that Figs. 12(a) and 12(b) show droplet velocities against time in categories C1 and C2 for the two different sprays mentioned and Figs. 12(c) and 12(d) show droplet momentum against time for the same droplets. By observing Figs. 12(a) and 12(b) one can see that C1 droplets and C2 droplets have different velocity profiles; i.e., the final values of C1 droplets velocities are normally higher, and they reach these values in a shorter time interval when compared to C2 droplets. If the droplets in both categories were to have similar masses, their momentum would be also categorized similarly. However, when their momentum is compared, there is no difference between both categories [Figs. 12(c) and 12(d)]. This situation is plausible if droplets in category C1 are smaller than droplets in category C2. If a rather similar charge level for every droplet is assumed (see Sec. III C), smaller droplets immersed in the same electric field would consequently accelerate more, but their momentum would not be significantly different. The similar inertia found for the droplets in the two different categories would be explained because droplet mass in case C2 balances the higher values found for droplet velocities in category C1. This assumption is supported by Fig. 13, which shows the calculated droplet diameters of both C1 and C2 droplets.

Figure 13 shows that droplets of category C1 have an average diameter of about 50 μm, while droplets in category C2 have an average diameter of about 100 μm; thus droplets of category C1 are indeed smaller than droplets of category C2. A direct consequence of this observation is that droplet inertia cannot be seen as a criterion to define whether situation case C1 or C2 will happen.

Contrary to that, the ligament breakup is an important factor that has to be considered because it defines both droplet size and position after polarization.

Following this line, it is now important to take some considerations into account in order to explain why C1 droplets are smaller than C2 droplets. First, it can be attributed to some oscillations normally found in infusion pumps, such as the one used in these experiments. Once the infused flow is not constant within a certain time frame, the jet volume will be also different with time, and different droplet sizes will appear after breakup. Second, the breakup process of the ligament is a very random phenomenon. Many external factors, which are responsible for the necessary perturbations needed to initiate the instabilities on the ligament surface, are directly influencing this breakup,

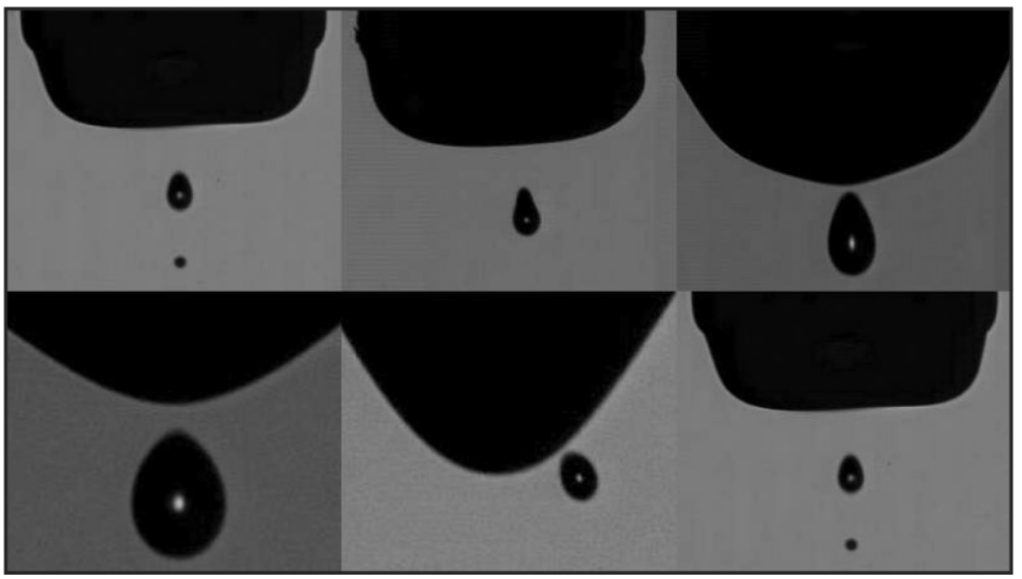

FIG. 11. Six examples of returning droplets assuming asymmetric tear shapes immediately before contacting the meniscus (this is not a sequence).

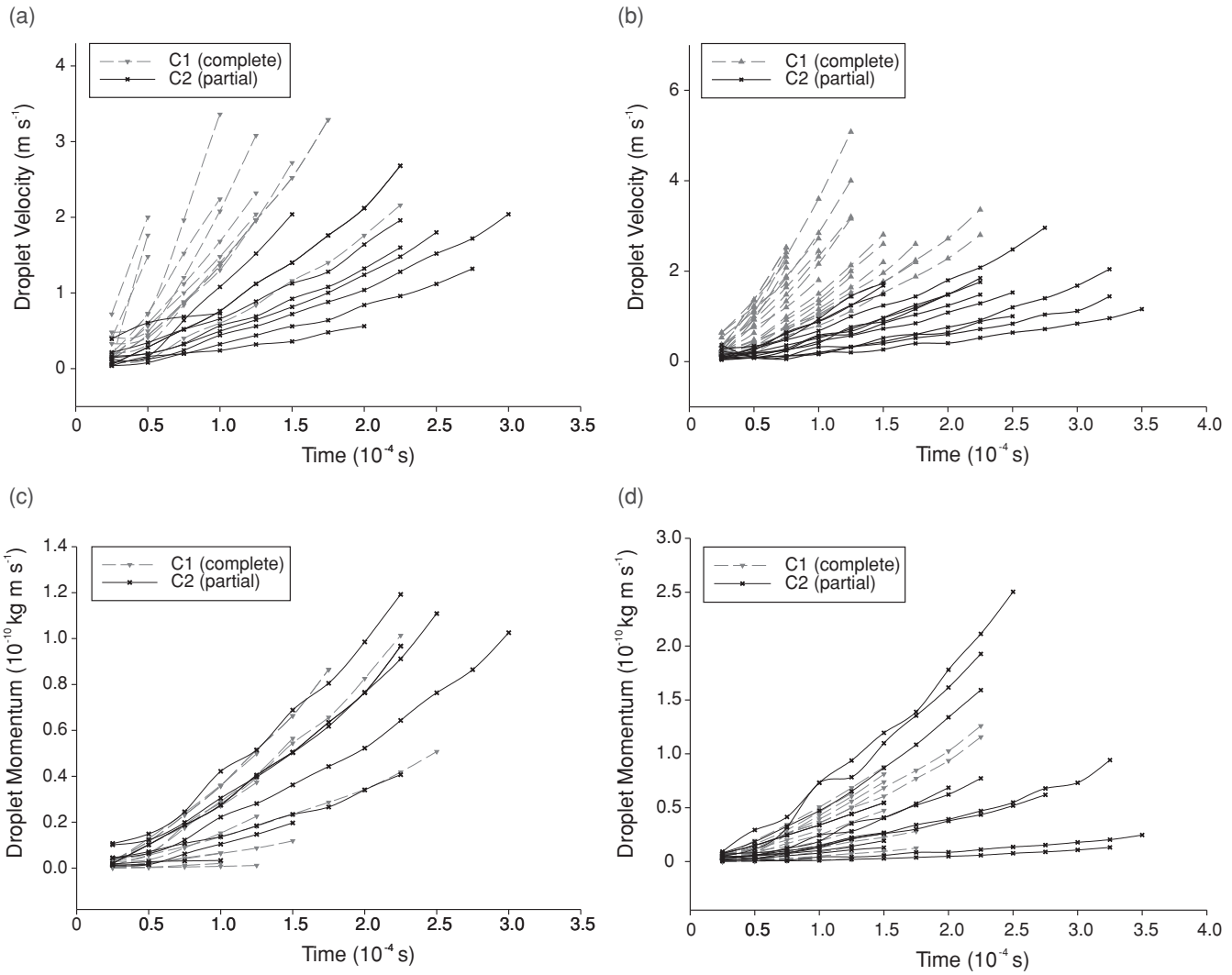

FIG. 12. (a) and (b) Droplet velocity against time in categories C1 and C2 for sprays of 0.5 mL h^{-1} and 2 mL h^{-1}. (c) and (d) Droplet momentum against time in categories C1 and C2 for the same sprays. Both sequences were recorded with 40 000 fps, which represents a time frame of 25 μs between two images. The flow and potential applied on the sprays represented in (a) and (c) are 0.5 mL h^{-1} and 6 kV, respectively, and are 2 mL h^{-1} and 5.5 kV on the sprays in (b) and (d).

e.g., ligament length, air currents, and electric field, and once we take this into account, it is not reasonable to assume that all the droplets will have similar diameters in this mode.

Since inertia does not make a difference on bouncing categories, we will consider the role of the electric field. In the case of deionized water, despite its high resistivity, hydraulic characteristic time cannot be shorter than electric characteristic time [45]. Nevertheless, we could see that droplets in category C1 were completely reintegrated, indicating that the hydraulic effect is dominating in this category. According to [25,28], the EF can provide bouncing of oppositely charged droplets, but there is a threshold to consider in this case for the magnitude of the EF. This would imply in our case that electric field values are consistently different for C1 and C2 droplets at the moment they approach the liquid meniscus. This can be explained if we look into the intrinsic behavior of the liquid meniscus in the pulsating jet mode. In this mode, the electric field oscillates continuously due to the change in space charge density, which is visible in the changing meniscus shape. For pulsating jet modes this oscillation period is rather constant. A direct consequence of these oscillations is the fact that, depending on how long the droplet takes to complete its returning movement, it approaches the meniscus in a period of higher or lower electric field strength. It is straightforward that a collision with a more conical meniscus would imply that the field strength on that moment is close to its maximum value. This hypothesis can be verified from Figs. 2 and 8 when, for the situation where the droplet is completely reintegrated to the meniscus (category C1, Fig. 2), the meniscus shape is still round and, for the partial coalescence situation (category C2, Fig. 8), the meniscus is more conical. Still, to test if this is true for all the other observed droplets we calculated the time interval the droplets remained in the air in each one of the mentioned categories, i.e., the droplet retention time. For C1 and C2 droplets the retention time is the time interval between the initial position after breakup and the last frame before contacting the meniscus. We also calculated the retention time for C3 droplets. In that case, since the droplet does not touch the meniscus, we define retention time as the time interval between

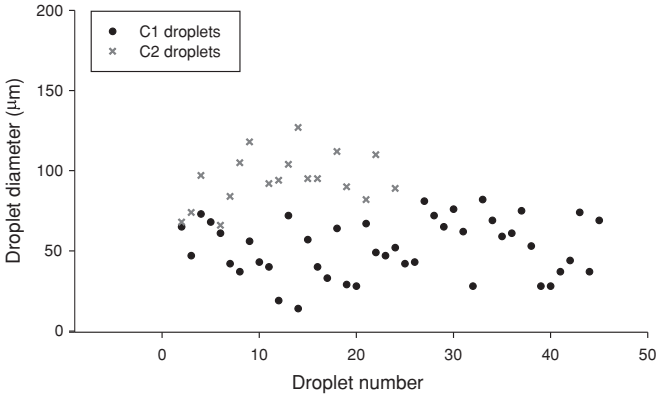

FIG. 13. Diameters of category C1 and C2 droplets for the sprays analyzed in Fig. 11

the initial position after breakup and the position immediately after the droplet leaves its equilibrium. The droplets were extracted from sprays with three different flow rates, 0.5, 1, and 2 mL h^{-1} in the pulsating jet mode. The droplet retention time can be used to have an idea if droplets will be exposed to a high electric field intensity for a prolonged time or not. In order to have a quantitative confirmation, we compared the droplet's retention time with the half period of the oscillation of the meniscus. It is clear from Fig. 14 that the retention time for the C2 case is closer to the half period than the C1 case. This means that C2 droplets are exposed to a higher electric field. It is important to note that the C3 case is even closer to the half period time; however, in this case the distance from meniscus to the droplets is much higher than in the other cases. As follows from the definitions of retention times, C3 cannot be directly compared to C1 and C2.

Looking now into category C3, a possible explanation for this situation would be the following: First, the droplet initial velocity is caused by the ligament downward momentum. After breakup the oppositely charged droplet starts its movement downward and stops. The meniscus deforms into a conical shape, i.e., the EF intensity increases. As the electric field

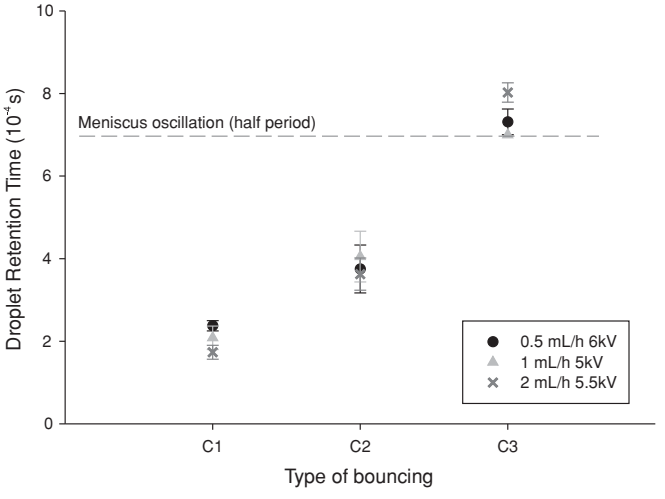

FIG. 14. Average retention time for droplets of categories C1, C2, and C3 for three different flow rates (0.5, 1, and 2 mL h^{-1}) compared with the average oscillation time of the liquid meniscus.

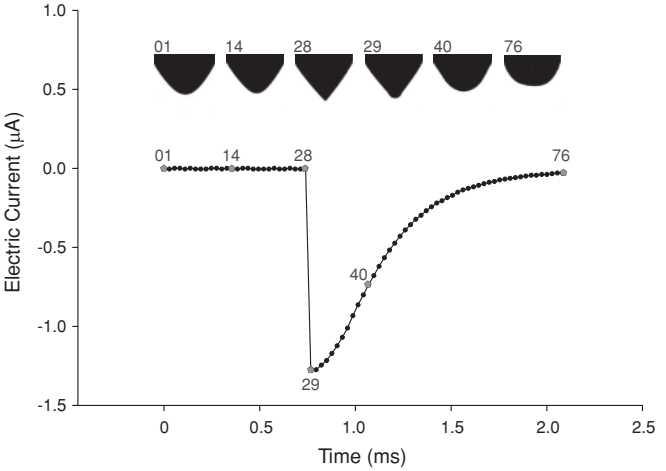

FIG. 15. Electric current against time synchronized with the spray movie. The spray flow was 1 mL h^{-1} with −5 kV applied on the counter electrode. The time frame between two images is 27 μs. The meniscus shape is represented by the images of some frames, and the respective electric current signal for each frame is presented in the plot.

intensity increases, the electric force balances droplet gravity, and the droplet reaches an equilibrium. The meniscus starts to retract, indicating a reduction of the EF intensity. Electric forces also decrease, and gravity moves the droplet downward again.

It was further noticed that the reason for the downward movement is not only gravity because the settling velocity of a droplet of this size is expected to be around 2.72×10^{-2} m s^{-1}, while our droplet moves with 1.2 m s^{-1}. This high velocity can be explained if the droplet has its charge inverted by a short electrical discharge originating from the cone tip [46]. This suggestion is corroborated by the fact that the droplet retention time is bigger than the half oscillation period, as can be seen in Fig. 14 and also in the current vs time graph shown in Fig. 15. Figure 15 shows a current peak at the moment that the meniscus assumes its conical shape, which indicates a possible electrical discharge.

IV. CONCLUSIONS

The presented experiments resembled classical EHDA: A dc electric field interacts with deionized water and creates an electrospray in different modes, dependent on the field strength. What was hitherto unknown, however, is that in the pulsating jet mode, polarization forces can create oppositely charged droplets, thus changing repulsion into attraction and making them return to the cone from which they were ejected. Once there, there are different possibilities: coalescence, partial coalescence, or noncoalescence. We found that the different categories depend on the retention time of the droplet in relation to the meniscus oscillation period, i.e., the changing of the electric field strength. We believe that these results can be used to better understand phenomena like the Lenard's effect [36] and the buildup of the electric field inside thunderstorm clouds [47].

ACKNOWLEDGMENTS

This work was performed in the TTIW-cooperation framework of Wetsus, Centre of Excellence for Sustainable Water Technology (http://www.wetsus.nl). Wetsus is funded by the Dutch Ministry of Economic Affairs, the European Union Regional Development Fund, the Province of Fryslân, the City of Leeuwarden and the EZ/Kompas program of the "Samenwerkingsverband Noord-Nederland." The industrial participants of Wetsus research theme "Salt" are highly acknowledged for their financial support. The authors would also like to thank Professor Jakob Woisetschläger (Graz University of Technology) and Adam D. Wexler (Wetsus) for their valuable contributions.

[1] W. Gilbert, *De Magnete, Magneticisque Corporibus, et de Magno Magnete Tellure* (London Excudebat Petrus Short, London, 1600).
[2] L. Rayleigh, Proc. R. Soc. London **28**, 1878 (1882).
[3] L. Rayleigh, Proc. R. Soc. London **29**, 71 (1879).
[4] J. Zeleny, Phys. Rev. **3**, 69 (1914).
[5] J. Zeleny, Phys. Rev. **10**, 1 (1917).
[6] G. Taylor, Proc. R. Soc. London Ser. A **313**, 453 (1969).
[7] J. Marijnissen, J. Aerosol Sci. **35**, 3 (2004).
[8] K. B. Geerse *et al*., J. Aerosol Sci. **30**, S553 (1999).
[9] K. B. Geerse and J. C. M. Marijnissen, in *Optimization of Aerosol Drug Delivery*, edited by L. Gradon and J. Marijnissen (Springer, Dordrecht, 2003), p. 75.
[10] C. U. Yurteri, J. C. M. Marijnissen, and R. P. A. Hartman, KONA Powder Part. J. **28**, 24 (2010).
[11] A. G. Bailey, *Electrostatic Spraying of Liquids* (Wiley, New York, 1988).
[12] J. M. Grace and J. C. M. Marijnissen, J. Aerosol Sci. **25**, 1005 (1994).
[13] J. Eggers and E. Villermaux, Rep. Prog. Phys. **71**, 036601 (2008).
[14] I. Marginean *et al*., Anal. Chem. **76**, 4202 (2004).
[15] M. Cloupeau and B. Prunet-Foch, J. Aerosol Sci. **25**, 1021 (1994).
[16] I. Marginean, P. Nemes, and A. Vertes, Phys. Rev. E **76**, 026320 (2007).
[17] R. S. Carson and C. D. Hendricks, AIAA J. **3**, 1460 (1964).
[18] R. Juraschek and F. W. Röllgen, Int. J. Mass Spectrom. **177**, 1 (1998).
[19] E. C. Fuchs *et al*., J. Phys. D **40**, 6112 (2007).
[20] E. C. Fuchs *et al*., Proc. SPIE **7376**, 73761E (2010).
[21] L. W. Armstrong, Electr. Eng. 154 (1893).
[22] H. T. Ochs and R. R. Czys, Nature (London) **327**, 606 (1987).
[23] P. Atten, J. Electrost. **30**, 259 (1993).
[24] R. S. Allan and S. G. Mason, J. Colloid Sci. **17**, 383 (1962).
[25] J. C. Bird *et al*., Phys. Rev. Lett. **103**, 164502 (2009).
[26] R. S. Allan and S. G. Mason, Trans. Farad. Soc. **57**, 2027 (1961).
[27] J. P. Borra *et al*., J. Aerosol Sci. **30**, 945 (1999).
[28] W. D. Ristenpart *et al*., Nature (London) **461**, 377 (2009).
[29] P. R. Brazier-Smith, Phys. Fluids **14**, 1 (1971).
[30] R. L. Grimm and J. L. Beauchamp, J. Phys. Chem. B **109**, 8244 (2005).
[31] M. A. Fontelos, U. Kindelan, and O. Vantzos, Phys. Fluids **20**, 092110 (2008).
[32] R. P. A. Hartman *et al*., J. Aerosol Sci. **30**, 823 (1999).
[33] R. P. A. Hartman *et al*., J. Aerosol Sci. **31**, 65 (2000).
[34] R. P. A. Hartman *et al*., J. Aerosol Sci. **29**, S977 (1998).
[35] R. P. A. Hartman, J. C. M. Marijnissen, and B. Scarlett, J. Aerosol Sci. **28**, S527 (1997).
[36] P. Lenard, Ann. Phys. (Weinheim, Germany) **8**, 149 (1902).
[37] D. C. Blanchard, J. Meteor. **15**, 383 (1958).
[38] J. T. Maze, T. C. Jones, and M. F. Jarrold, J. Phys. Chem. A **110**, 12607 (2006).
[39] A. M. Ganan-Calvo and J. M. Montanero, Phys. Rev. E **79**, 066305 (2009).
[40] A. A. Zavitsas, J. Phys. Chem. B **105**, 7805 (2001).
[41] R. Hartman, Ph.D. thesis, Nanostructured Materials Department, Delft University of Technology, Delft, The Netherlands, 1998, p. 178.
[42] A. T. Blades, M. G. Ikonomou, and P. Kebarle, Anal. Chem. **63**, 2109 (1991).
[43] K. B. Geerse, Ph.D. thesis, Nanostructured Materials Department, Delft University of Technology, Delft, The Netherlands, 2003, p. 138.
[44] W. C. Hinds, *Aerosol Technology*, 2nd ed. (Wiley-Interscience, New York, 1998)
[45] U. Stachewicz *et al*., Langmuir **25**, 2540 (2009).
[46] R. A. Roos, Dr. 2011: Nocé, France (personal communication).
[47] C. Saunders, Space Sci. Rev. **137**, 335 (2008).